

Quasi-geostrophic diagnosis of the influence of vorticity advection on the development of upper level jet-front systems

Jonathan E. Martin*

Department of Atmospheric and Oceanic Sciences, University of Wisconsin-Madison, WI, USA

*Correspondence to: J. E. Martin, Department of Atmospheric and Oceanic Sciences, University of Wisconsin-Madison, 1225 W. Dayton St, Madison, WI 53705, USA. E-mail: jemart1@wisc.edu

A partition of the geostrophic vorticity into shear and curvature components is employed to consider the influence of differential vorticity advection on the development of upper level jet-front systems in northwesterly flow in an idealized and an observed case. The analysis reveals that negative geostrophic shear vorticity advection by the thermal wind, inextricably coincident with regions of geostrophic cold air advection in cyclonic shear, forces subsidence that is distributed in narrow, quasi-linear, frontal-scale bands aligned along the warm edge of the upper baroclinic zone. In each case examined, this component of the quasi-geostrophic (QG) subsidence makes the largest contribution to upper frontogenetic tilting.

Additionally, since QG omega forced by geostrophic vorticity advection by the thermal wind is of the shearwise variety, the analysis shows that the traditional emphasis on the role of laterally displaced transverse circulations is an incomplete description of the upper frontogenetic tilting that arises in such environments. In fact, the results suggest that Mudrick's (1974) emphasis on negative vorticity advection increasing with height combined with Shapiro's (1981) insight regarding the lateral displacement of frontogenetic transverse circulations offers the most comprehensive way to conceptualize the forcings that promote rapid upper level jet-front development in regions of geostrophic cold air advection in cyclonic shear.

Key Words: upper level jet-fronts; vorticity advection; tilting

Received 24 July 2013; Revised 7 January 2014; Accepted 8 January 2014; Published online in Wiley Online Library 26 March 2014

1. Introduction

Careful analysis of radiosonde observations of the upper troposphere by Reed and Sanders (1953), Newton (1954), Reed (1955), and Reed and Danielsen (1959) revealed the existence of upper tropospheric frontal structures that were essentially independent of the more conventional surface-based frontal zones first emphasized in the Norwegian Cyclone Model (Bjerknes and Solberg, 1922). These upper-level fronts were found to be of synoptic-scale length but mesoscale width and characterized by locally strong horizontal and vertical shear like their surface-based counterparts. It was hypothesized in these contributions that differential vertical motion, with subsidence preferentially on the warm side of an upper-level baroclinic zone, was responsible for tilting vertical shear and vertical potential temperature gradients into the horizontal. Additional evidence for the centrality of tilting in the genesis of upper-level fronts was the fact that these features routinely exhibited downward extrusions of stratospheric air (manifest in high values of potential vorticity (PV) as well as radioactivity) into the upper troposphere beneath the tropopause-level jet core (Reed and Danielsen, 1959).

The importance of understanding the processes by which these upper-level fronts develop derives from their influence on a number of important meteorological phenomena. By virtue of their association with extrusion of stratospheric PV into the middle and upper troposphere, upper fronts have been examined as the progenitors of the mid-tropospheric waves (i.e. vorticity maxima) directly associated with lower-tropospheric development (e.g. Uccellini *et al.*, 1985; Sanders, 1988; Lackmann *et al.*, 1997). Upper fronts are also primary conduits of stratospheric/tropospheric exchange (e.g. Danielsen, 1964; Shapiro, 1980; Stohl *et al.*, 2003). Finally, the upper frontogenesis process involves substantial deformation of the tropopause, both above and below the jet core and so contributes to the structure and evolution of lower-stratospheric frontal zones (Lang and Martin, 2012).

Much of the work regarding upper frontal development since the pioneering studies of the 1950s has considered the synoptic-scale environments within which the requisite differential vertical motions might develop. Three-dimensional channel models of growing baroclinic waves repeatedly show that the phase difference between the pressure and thermal waves results in a tendency for geostrophic cold air advection along the downstream portions of upper-level baroclinic zones in northwesterly flow

(e.g. Mudrick, 1974; Buzzi *et al.*, 1977; Newton and Trevisan, 1984; Rotunno *et al.*, 1994).

Mudrick (1974) examined the upper frontogenesis process in northwesterly flow using the output from an idealized channel model. Employing both quasi-geostrophic (QG) and primitive equation (PE) simulations, he found that in both cases the strongest descent in the middle and upper troposphere was located beneath the jet core. This subsidence contributed to the tilting of isentropes as well as horizontal vortex tubes in such a way as to intensify the horizontal temperature contrast and sharpen the jet. Mudrick diagnosed the frontogenetic subsidence as resulting from a combination of vorticity advection decreasing with height* and the subsidence branch of a thermally direct vertical circulation associated with confluent frontogenesis. It is clear that, though he references this combination of forcings, the predominant forcing in the Mudrick conceptual model is the vorticity advection. Indeed, he argued that subsidence through the jet core, via tilting, serves to increase the cross-jet vorticity gradient by simultaneously increasing (decreasing) the relative vorticity on the cyclonic (anticyclonic) shear side, thus providing an environment in which the negative vorticity advection (NVA) driving the subsidence might be intensified. A similar positive feedback mechanism was diagnosed for a hierarchy of approximations by Keyser and Pecnick (1985) and Reeder and Keyser (1988).

Shapiro (1981, 1983) considered the effect of both confluence and horizontal shear on upper frontogenesis from the perspective of the Sawyer (1956) – Eliassen (1962) circulation equation. He argued that the effect of horizontal shear on a positive along-front thermal gradient (i.e. geostrophic cold air advection) was to displace the thermally direct circulation associated with the confluent frontogenesis toward the warm side of developing upper fronts (Rotunno *et al.* (1994) referred to this as the Shapiro effect). Such lateral displacement placed the subsidence branch of the circulation on the warm side of the upper baroclinic zone, promoted frontogenetic tilting, and gave it the appearance of being thermally indirect.

Keyser and Pecnick (1985) employed a two-dimensional primitive equation model to investigate quantitatively the effect of this combination of confluence and horizontal shear on the development of fronts near the tropopause. They found that in the case of geostrophic cold air advection in cyclonic shear, a well-defined front developed first at the tropopause and then extended into the mid-troposphere. This development was dominated by tilting provided by a circulation that was interpreted as a thermally direct cross-front ageostrophic circulation displaced far enough into the warm air to place the maximum subsidence in the mid-troposphere within and to the warm side of the developing frontal zone. A noteworthy result of this work was that, despite its purely two-dimensional (2D) approach, the resulting structures closely resembled those discovered in the aforementioned observational studies. In other words, the effect of flow curvature on the resulting vertical motion field was not required to reproduce realistic frontal structures.

The theoretical/observational studies of Shapiro and the modelling studies of Keyser and collaborators (e.g. Keyser and Pecnick, 1985; Keyser and Shapiro, 1986; Reeder and Keyser, 1988; Pecnick and Keyser, 1989; Keyser *et al.*, 1992a; Keyser, 1999) focus on upper frontogenetic tilting forced by transverse† circulations that arise from horizontal frontogenesis (frontolysis) associated

with confluence and horizontal shear. In these studies, which have contributed greatly to modern understanding of the upper frontogenesis process, the lateral shift of these transverse circulations toward the warmer or colder air has been emphasized. An unintended, but nonetheless unfortunate, consequence of this focus has been a lack of emphasis on the role of differential vorticity advection in the upper frontogenesis process as outlined by Mudrick (1974). Vorticity advection by the thermal wind is a component of what Martin (2006) referred to as the shearwise omega (ω_s). Since ω_s is forced by convergence of the along-isentrope component of the \mathbf{Q} -vector (Hoskins *et al.*, 1978), it is associated with the rotation of $\nabla\theta$ (often referred to as ‘rotational frontogenesis’), not changes in its magnitude (Keyser *et al.*, 1992b). Henceforth, ‘frontogenesis’ will refer only to the process of changing $|\nabla\theta|$. In this article we show that the Shapiro effect – operation of horizontal shear on a positive along-front thermal gradient – is associated with a vertical circulation that responds to both frontogenesis and vorticity advection by the thermal wind which are physically distinct forcings. In fact, it is demonstrated that the predominant sinking motion that drives upper frontogenesis in such synoptic environments can be related to negative geostrophic shear vorticity advection by the thermal wind.

The article is organized in the following manner. A review of the nature of shearwise and transverse QG vertical motions is given in section 2. As a component of that review it is demonstrated that vorticity advection by the thermal wind is a distinctly shearwise species of QG vertical motion. Also in section 2, the partition of the geostrophic vorticity into its shear and curvature components is described and a method for calculating the QG vertical motions associated with each portion of the vorticity is presented. Section 3 contains analyses of two cases – one an idealized numerical simulation, the other an observed case – that demonstrate the influence of shear vorticity advection by the thermal wind on the development of upper level jet-front systems. Conclusions are presented in section 4 along with discussion of the results and suggestions for future work.

2. Theoretical background and methodology

2.1. Vertical motions associated with jet streaks

Keyser *et al.* (1992b) demonstrated that the total quasi-geostrophic (QG) vertical motion could be partitioned into orthogonal portions associated with the across- and along-isentrope \mathbf{Q} -vector divergence, ω_n and ω_s , respectively. They concluded that the characteristic comma-shaped vertical motion distribution of the midlatitude cyclone arises from the modification of a cellular (ω_s) dipole pattern by the banded (ω_n) dipoles associated with frontal zones. It is important to note that ω_n is precisely the vertical motion associated with geostrophic frontogenesis. To emphasize their orientations to the thermal wind (i.e. the geostrophic vertical shear), Martin (2006) referred to ω_s and ω_n as the shearwise (along shear) and transverse (across shear) QG vertical motions, respectively. He demonstrated that lower-tropospheric cyclogenesis responds predominantly to column stretching associated with the updraught portion of the shearwise QG vertical motion.

This suggestion is consistent with the insight of Sutcliffe (1947) who demonstrated that a significant portion of the synoptic-scale upward vertical motion could be attributed to cyclonic vorticity advection by the thermal wind ($-\mathbf{V}_T \cdot \nabla \zeta_g$). Since the geostrophic wind is non-divergent on an f -plane, this is equivalent to the flux divergence of the vector $\mathbf{V}_T \zeta_g$ which, by definition, is aligned parallel to the geostrophic vertical

*Specifically, Mudrick (1974) indicates ‘... a region of NVA, the magnitude of which increases with height below the jet core ...’.

†Here, *transverse* refers to couplets of ascent and descent that straddle the geostrophic flow.

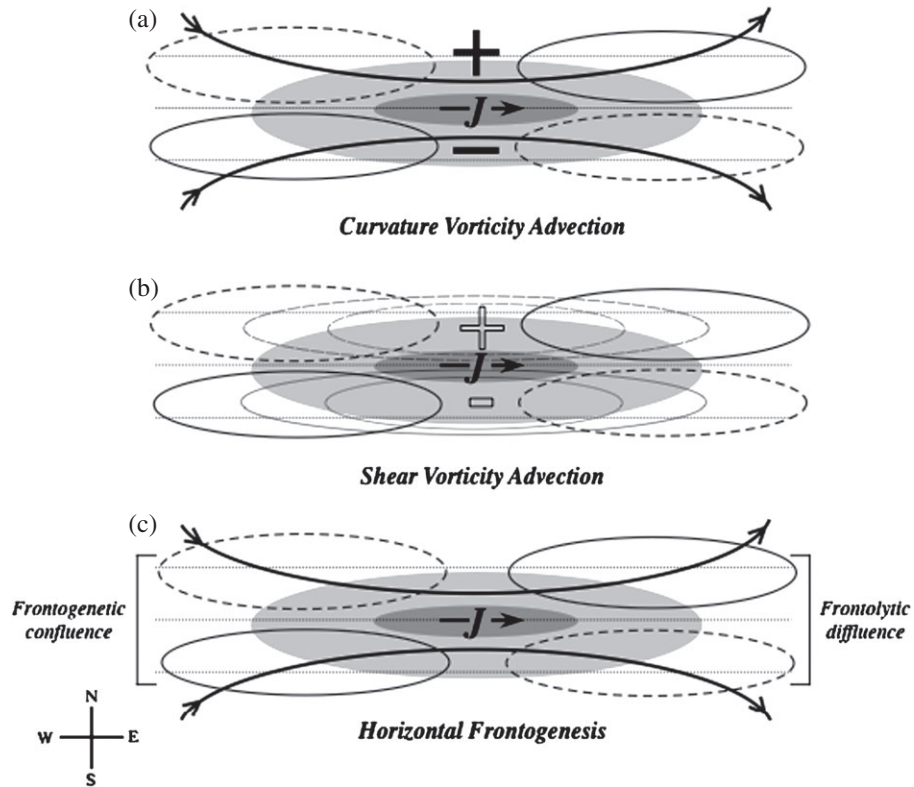


Figure 2. Schematic straight jet streak with no along-flow geostrophic temperature advection illustrating the vertical circulations associated with (a) geostrophic curvature advection by the thermal wind, (b) geostrophic shear vorticity advection by the thermal wind, and (c) horizontal frontogenesis. Shading represents isotachs with 'J' indicating the jet core. Dotted lines are isentropes with colder air to the north. Medium solid (dashed) lines are regions of quasi-geostrophic (QG) ascent (descent). In (a) and (c) the bold solid lines are geopotential height lines while in (b) the thin dashed (solid) lines represent schematic contours of positive (negative) geostrophic shear vorticity.

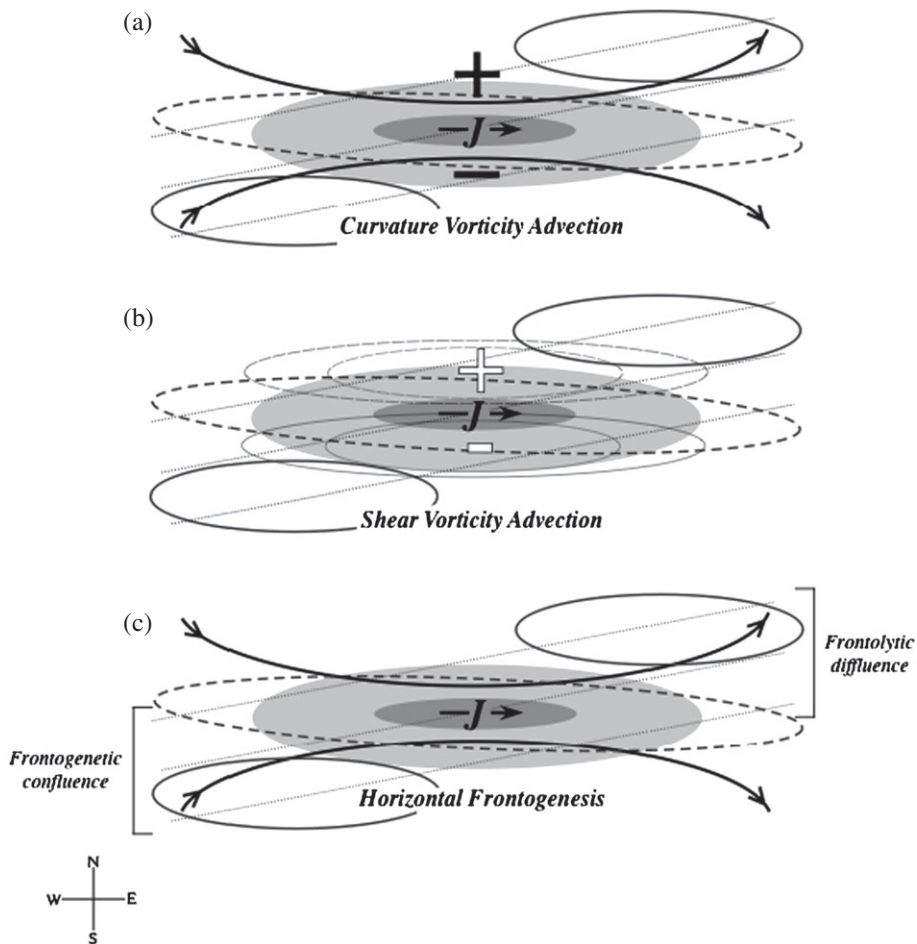


Figure 3. As for Figure 2 except for a straight jet characterized by geostrophic cold air advection along its length.

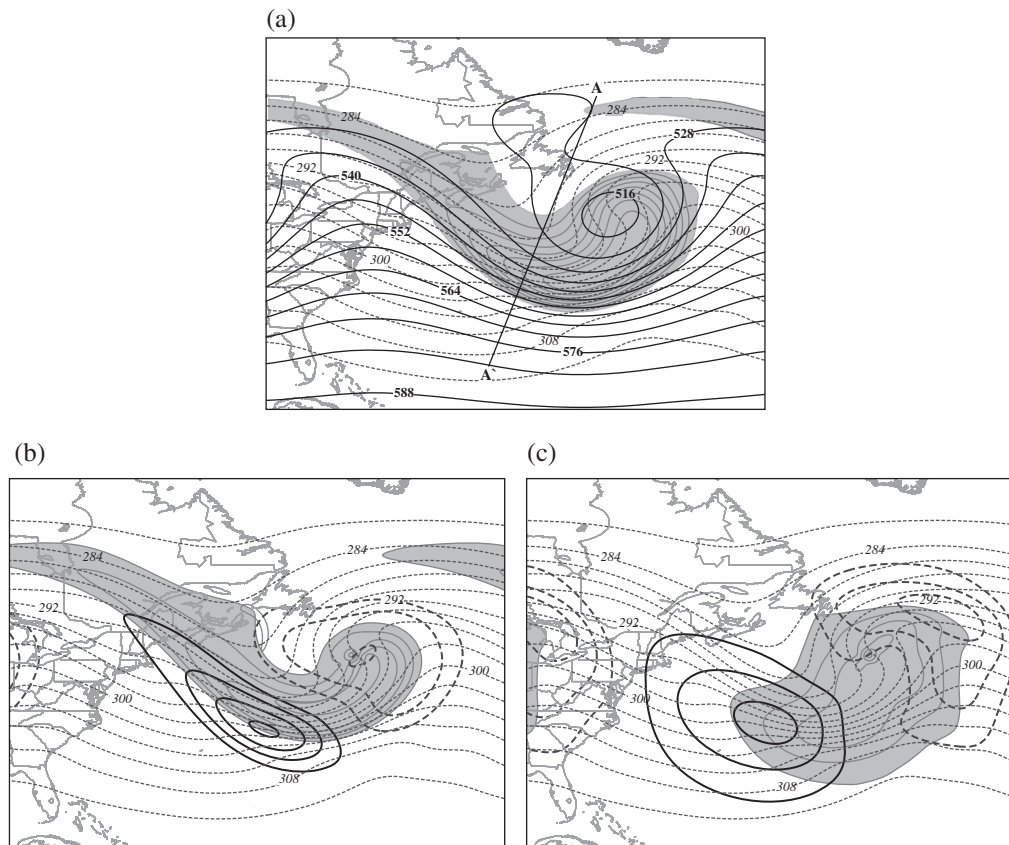


Figure 4. (a) 36 h forecast of 500 hPa geopotential height (bold solid lines), potential temperature (dashed lines) and geostrophic vorticity (shaded and labelled) from the idealized UW-NMS simulation. Vorticity labelled and contoured in units of $2 \times 10^{-5} \text{ s}^{-1}$, beginning at $2 \times 10^{-5} \text{ s}^{-1}$. Geopotential height labelled in m and contoured every 60 m. Potential temperature labelled in K and contoured every 2 K. Vertical cross-sections along line A–A' are shown in Figure 5. (b) 36 h forecast of 500 hPa geostrophic shear vorticity, potential temperature, and QG ω associated with geostrophic shear vorticity advection by the thermal wind from the UW-NMS idealized simulation. Vorticity shaded and contoured as in (a). Potential temperature labelled and contoured as in (a). Solid (dashed) lines are 500 hPa QG ω contoured every 1 (–1) dPa s^{-1} starting at 1 (–1) dPa s^{-1} . (c) As for (b) but for geostrophic curvature vorticity and QG ω associated with geostrophic curvature vorticity advection by the thermal wind. Continents are included only for scale.

in Figure 3, that location is shifted to the southern side of the jet entrance region and to the northern side of the jet exit region (Figure 3(c)). As a consequence, the thermally direct entrance (indirect exit) region circulation is shifted southward (northward) such that the subsidence branch is located over the jet core. Once again, these three components of the total vertical motion are distributed in such a way as to encourage a single, subsiding current through the jet core, a circulation that has been shown to be central to the development of upper level jet-front systems (e.g. Keyser and Pecnick, 1985). It is a straightforward extrapolation of the above argument to note that for jet streaks of synoptic-scale length (where the radius of curvature in the geopotential height contours is large), curvature vorticity advection will make a meagre contribution to the vertical motions. Importantly, this schematic analysis affirms that the vertical circulation that drives upper frontogenetic tilting is composed of both shearwise and transverse components – a conceptual departure from the singular emphasis on transverse circulations that has dominated the investigation of upper frontogenetic tilting in the previous literature. The goal of this article is to determine the relative contributions to upper frontogenesis made by each component.

2.2. Calculation of QG omega

In the subsequent section, gridded analyses from the National Center for Environmental Prediction's (NCEP's) Global Forecast System (GFS) model as well as output from an idealized simulation of the University of Wisconsin Non-hydrostatic Modeling System (UW-NMS: Tripoli, 1992) are used in the calculation of the

QG omega. The idealized simulations were carried out using an adiabatic channel model version of the UW-NMS (Tripoli, 1992) employing an analytic initialization scheme based upon formulations by Fritsch *et al.* (1980), Nuss and Anthes (1987), and Cao and Cho (1995). The simulations were run on a spherical grid with resolution $126 \times 100 \text{ km}$ at the Equator over a domain $5800 \times 6000 \text{ km}$ centred at 38°N . Forty vertical levels were used with dz starting at 300 m and stretching to 600 m above the first 12 grid levels. The model top (at 20.5 km) included a Rayleigh friction zone while the bottom was flat and homogeneous with a Businger surface layer. A first-order turbulence closure scheme was used. The initialization specifies a zonal jet with a 4000 km moderate amplitude sinusoidal perturbation in temperature and pressure imposed upon it, along with a height invariant lateral shear[†] of $4.5 \times 10^{-5} \text{ s}^{-1}$ similar to that used in the LC2 experiments of Thorncroft *et al.* (1993). The integrations were run for 96 h.

In the calculation of omega, the gridded analyses from the GFS and forecast output from the UW-NMS are first bilinearly interpolated from their original output grids to a $1^\circ \times 1^\circ$ latitude/longitude grid at 19 isobaric levels from 1000 to 100 hPa at 50 hPa increments using an interpolation program included in the General Meteorology Package (GEMPAK). The grid-point height and temperature data were then subjected to a Gaussian smoother that eliminates roughly two-thirds of the energy at

[†]A domain-wide, barotropic shear of 20 m s^{-1} was distributed over 40° of latitude (from 20°N to 60°N).

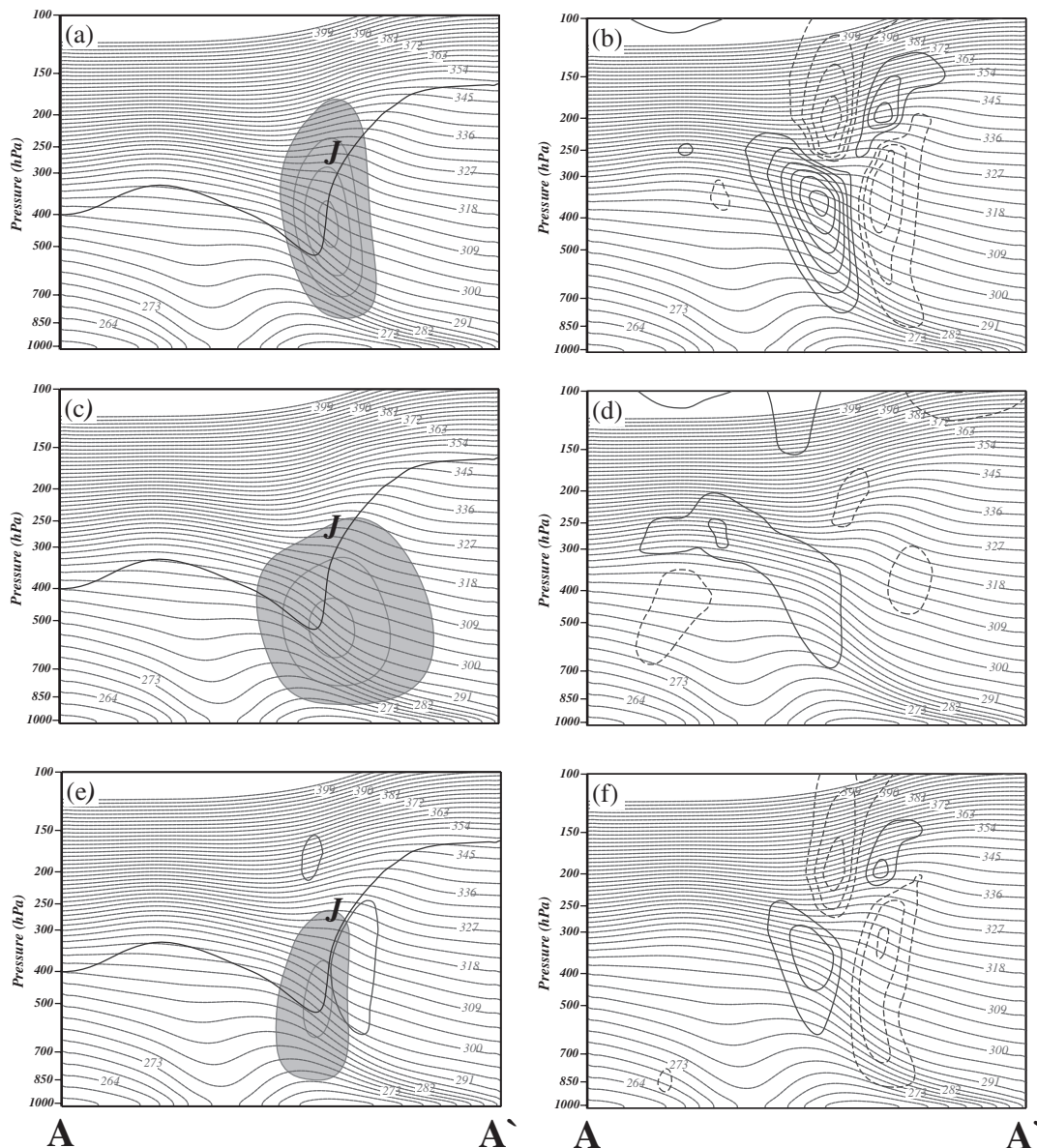


Figure 5. (a) Vertical cross-section along A–A' in Figure 4(a) of potential temperature (dashed thin lines), QG subsidence associated with geostrophic shear vorticity advection by the thermal wind (shaded) and the dynamic tropopause (bold line) from the 36 h forecast of the UW-NMS idealized simulation. Potential temperature is labelled in K and contoured every 3 K. 'J' indicates the position of the jet core. QG subsidence contoured every 1 dPa s⁻¹ starting at 1 dPa s⁻¹. (b) Vertical cross-section along A–A' in Figure 4(a) of potential temperature (labelled and contoured as in (a)) and tilting frontogenesis associated with the QG subsidence in (a) from the 36 h forecast of the UW-NMS idealized simulation. Thick solid (dashed) lines are positive (negative) tilting frontogenesis contoured every 2 (–2) × 10⁻¹⁰ K m⁻¹ s⁻¹ starting at 2 (–2) × 10⁻¹⁰ K m⁻¹ s⁻¹. (c) As for (a) but with shading representing QG subsidence associated with curvature vorticity advection by the thermal wind. (d) As for (b) but with tilting frontogenesis associated with the subsidence in (c). (e) As for (a) but shading representing QG subsidence associated with geostrophic horizontal frontogenesis (bold solid lines). Geostrophic frontogenesis contoured every 5 × 10⁻⁹ K m⁻¹ s⁻¹ starting at 5 × 10⁻⁹ K m⁻¹ s⁻¹. (f) As for (b) but with tilting frontogenesis associated with the subsidence in (e).

wavelengths ≤660 km, yielding results similar to those achieved using the cowbell filter described by Barnes *et al.* (1996) for use in quasi-geostrophic diagnostics with mesoscale models. Employing the technique of successive over-relaxation (SOR),

$$= -2\nabla \cdot \mathbf{Q} \tag{5a}$$

$$= -2\nabla \cdot \mathbf{Q}_n \tag{5b}$$

$$\sigma \left(\nabla^2 + \frac{f_o^2}{\sigma} \frac{\partial^2}{\partial p^2} \right) \omega = -2\nabla \cdot \mathbf{Q}_s \tag{5c}$$

$$= -2\nabla \cdot \mathbf{Q}_{TR_{curv}} \tag{5d}$$

$$= -2\nabla \cdot \mathbf{Q}_{TR_{shear}} \tag{5e}$$

the *f*-plane version of the QG omega equation is solved using a spatially averaged static stability that varies for each time with *f*_o set equal to the central latitude of the domain for each of the cases examined. With geostrophic forcing corresponding to the divergences of **Q**, **Q_n** and **Q_s**, the total (Eq. (5a)),

transverse (Eq. (5b)) and shearwise (Eq. (5c)) QG vertical motions, respectively, are returned in units of Pa s⁻¹. Those portions of the shearwise QG omega associated with curvature and shear vorticity advection by the thermal wind are calculated separately using Eq. (5d) and Eq. (5e), respectively. The author knows of no prior study that has separately calculated these last two species of the QG omega. Next, the separate roles of shear and curvature vorticity advection by the thermal wind as well as horizontal confluence/diffuence in the production of vertical motions that accomplish upper frontogenetic tilting in the real observed case as well as the idealized simulation are considered.

3. Analysis

In this section, two cases of upper frontogenesis in northwesterly flow are explored. The analysis begins with examination of the idealized simulation.

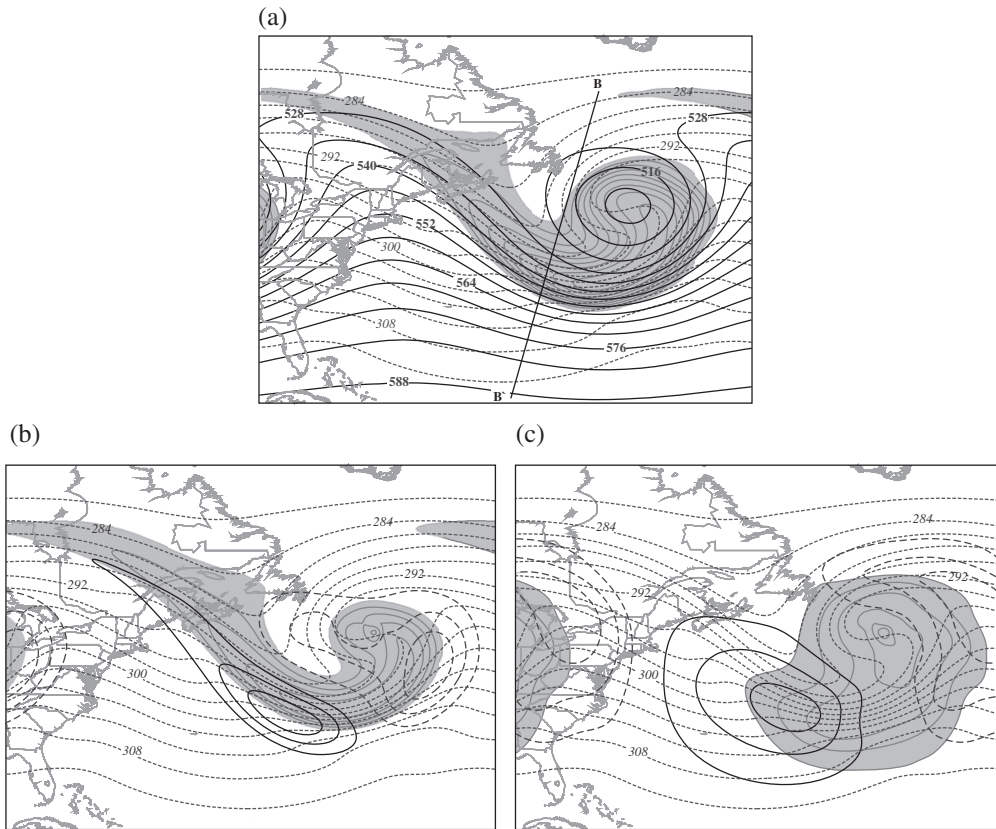


Figure 6. (a) As for Figure 4(a) but from a 42 h forecast of the UW-NMS idealized simulation. Vertical cross-sections along line B–B' are shown in Figure 7. (b) As for Figure 4(b) but from a 42 h forecast of the UW-NMS idealized simulation. (c) As for Figure 4(c) but from a 42 h forecast of the UW-NMS idealized simulation.

3.1. Idealized UW-NMS simulation

The 500 hPa analysis from the 36th hour of the idealized simulation, hereafter referred to as H36, is shown in Figure 4. The geopotential height and temperature structure in Figure 4(a) demonstrates the phase lag between the geopotential trough and the thermal trough that Shapiro (1981) argued is characteristic of developing baroclinic waves. The consequence of this phase shift in the model cyclone is the substantial region of geostrophic cold air advection which begins just downstream of the ridge crest and continues through the entire length of the trough axis to the downstream thermal ridge axis. Isopleths of the geostrophic vorticity at 500 hPa are also included in Figure 4(a). The orientation of isentropes to isopleths of vorticity demonstrates that from the ridge crest to approximately the base of the trough axis, there is negative vorticity advection by the thermal wind. It also appears that the maximum NVA by the thermal wind is located on the warm side of the 500 hPa baroclinic zone. More precise insight into the distribution of the geostrophic vorticity and the associated QG omega is obtained by partitioning the total vorticity into its shear and curvature components.

The QG omega forced by shear vorticity advection (Figure 4(b)) shows a quasi-linear band of maximum subsidence with its axis precisely along the warm edge of the upper baroclinic zone. A similar analysis employing the geostrophic curvature vorticity is shown in Figure 4(c). Here the maximum NVA by the thermal wind is located just upstream of the trough axis and does not exhibit a strong bias toward one side of the baroclinic zone or the other. The resulting subsidence region is more kidney bean-shaped in nature with its long axis displaced slightly toward the warm side of the upper baroclinic zone.

A vertical cross-section along A–A' in Figure 4(a) reveals the distribution of the various subsidence maxima associated with the upper frontal development at this time. Shear vorticity

advection by the thermal wind forces a narrow, fairly intense downdraught, centred just equatorward of the steepest portion of the dynamic tropopause (indicated by the 1.5 PVU isopleth of potential vorticity) and on the warm side of the upper tropospheric baroclinic zone (Figure 5(a)). This subsidence forces notable tilting frontogenesis ($F_{\text{tilt}} = -\frac{\partial \theta}{\partial p} \frac{\partial \omega}{\partial n}$ where \hat{n} points into the cold air) in the developing upper frontal zone (Figure 5(b)). A substantially different distribution of subsidence, associated with curvature vorticity advection, is shown in Figure 5(c). This more isotropic distribution, centred at a lower elevation, does considerably less tilting frontogenesis than that associated with shear vorticity advection (Figure 5(d)). Finally, the QG vertical motion associated with geostrophic horizontal frontogenesis (referred to as ω_n by Keyser *et al.* (1992b) and transverse ω by Martin (2006)) responds to the presence of a horizontal frontogenesis maxima displaced to the warm side of the upper baroclinic zone and exhibits a similar geometry to the subsidence associated with the shear vorticity advection (Figure 5(e)) with smaller magnitude and displacement further toward the cold side of the upper baroclinic zone. Consequently, although the QG frontogenetic transverse circulation does contribute to tilting frontogenesis (Figure 5(f)), it does less than 30% as much tilting as the subsidence associated with the shear vorticity advection.

The relative contributions of the various categories of QG subsidence remain the same at a later time in the development of the idealized storm. At H42, both the thermal and vortex structures of the storm are more intense. The 500 hPa geopotential and temperature analysis at H42 (Figure 6(a)) illustrates the continued presence of geostrophic cold air advection in the northwesterly flow from roughly the ridge crest to the eastern flank of the closed upper low. Once again, the region of strongest negative vorticity advection by the thermal wind is along the warm edge of the upper baroclinic zone and most of that is related to the shear vorticity (Figure 6(b)). The result of this

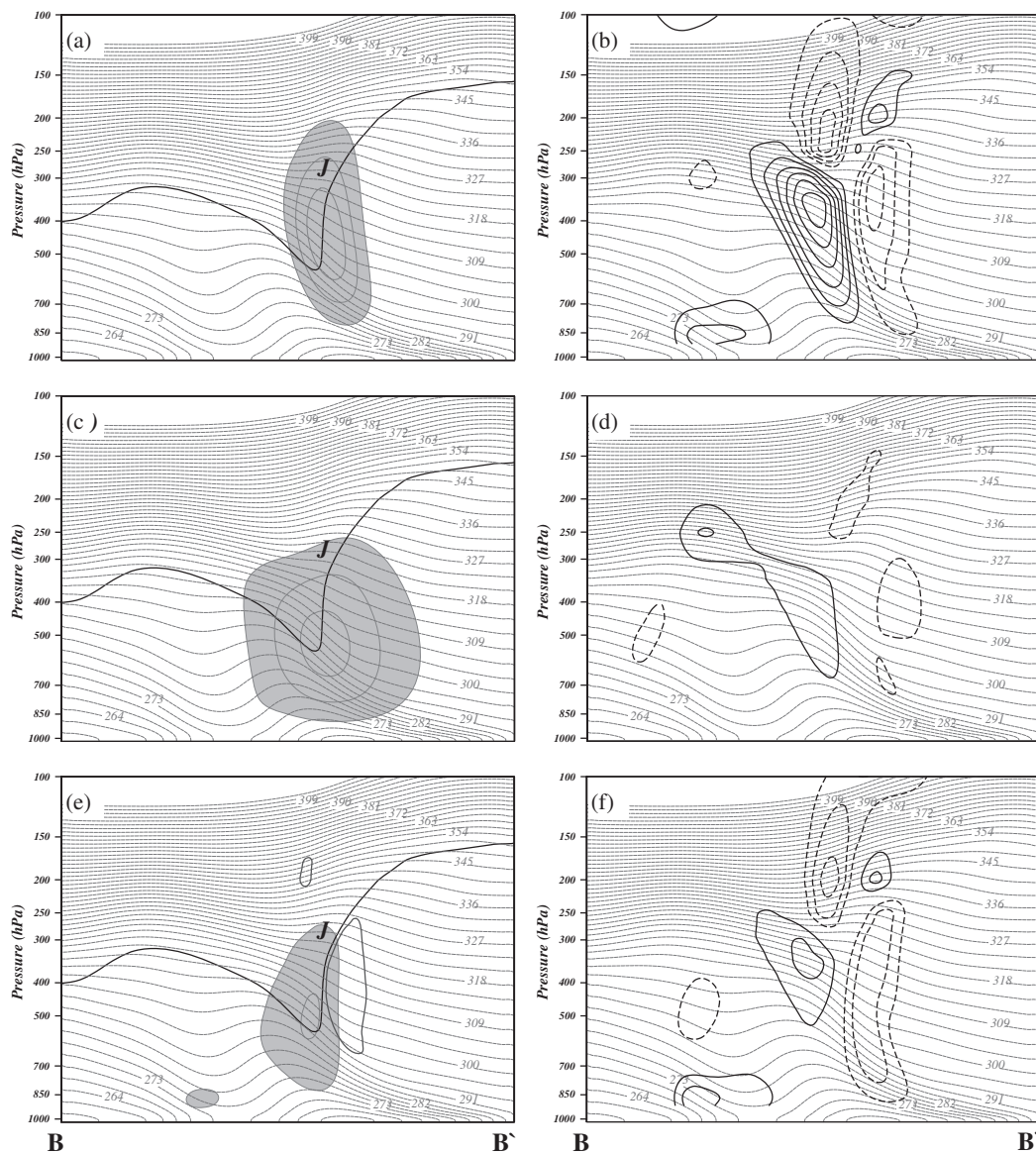


Figure 7. (a) As for Figure 5(a) but along B–B' in Figure 6(a) with data from the 42 h forecast of the UW-NMS idealized simulation. (b) As for Figure 5(b) but along B–B' in Figure 6(a) with data from the 42 h forecast of the UW-NMS idealized simulation. (c) As for Figure 5(c) but along B–B' in Figure 6(a) with data from the 42 h forecast of the UW-NMS idealized simulation. (d) As for Figure 5(d) but along B–B' in Figure 6(a) with data from the 42 h forecast of the UW-NMS idealized simulation. (e) As for Figure 5(e) but along B–B' in Figure 6(a) with data from the 42 h forecast of the UW-NMS idealized simulation. (f) As for Figure 5(f) but along B–B' in Figure 6(a) with data from the 42 h forecast of the UW-NMS idealized simulation.

forcing is an even more elongated linear band of subsidence on the warm edge of the upper front (Figure 6(b)). The curvature vorticity contribution looks nearly identical to that from H36 with a nearly identical distribution of associated QG vertical motion (Figure 6(c)).

Vertical cross-sections of QG ω and associated tilting frontogenesis along B–B' in Figure 6(a) are shown in Figure 7. As before, the subsidence associated with shear vorticity advection is centred on the warm side of the upper baroclinic zone just equatorward of the PV extrusion, is restricted horizontally, and lies beneath the jet core (Figure 7(a)). The associated tilting frontogenesis is very strong throughout the middle and upper troposphere (Figure 7(b)). The subsidence associated with the curvature vorticity advection is centred at a lower elevation, is more isotropic in shape, and more or less centred on the upper baroclinic zone (Figure 7(c)). Consequently, this subsidence does very little tilting frontogenesis (Figure 7(d)). Finally, the QG transverse circulation (Figure 7(e)) is nearly centred on the upper baroclinic zone as well and is fairly weak. Its associated tilting frontogenesis is both weak and restricted to the upper troposphere (Figure 7(f)).

3.2. Observed case: 8 April 2013

An intense upper level jet-front system developed in northwesterly flow just off the west coast of North America on 8 April 2013. This event is fairly representative of northwesterly flow cases that affect western and central North America during the cold season (Lang and Martin, 2013a). At 0000 UTC 8 April, the baroclinic zone involved in the frontogenesis was clearly evident at 500 hPa and had a geostrophic vorticity maximum along its entire length (Figure 8(a)). Modest geostrophic cold air advection was restricted to the southwest quadrant of the cut-off geopotential low near where the flow was strongly curved.

The 500 hPa QG ω associated with the geostrophic shear vorticity advection exhibited a quasi-linear subsidence feature stretching from northern coastal British Columbia southward to off the Oregon/California border (Figure 8(b)) where the subsidence was maximized on the warm side of the upper baroclinic zone (such was not the case along the northern portion of the subsidence region). Note the substantially isotropic distribution of the associated QG ascent to the southeast. The QG ω associated with the curvature vorticity was focused off the

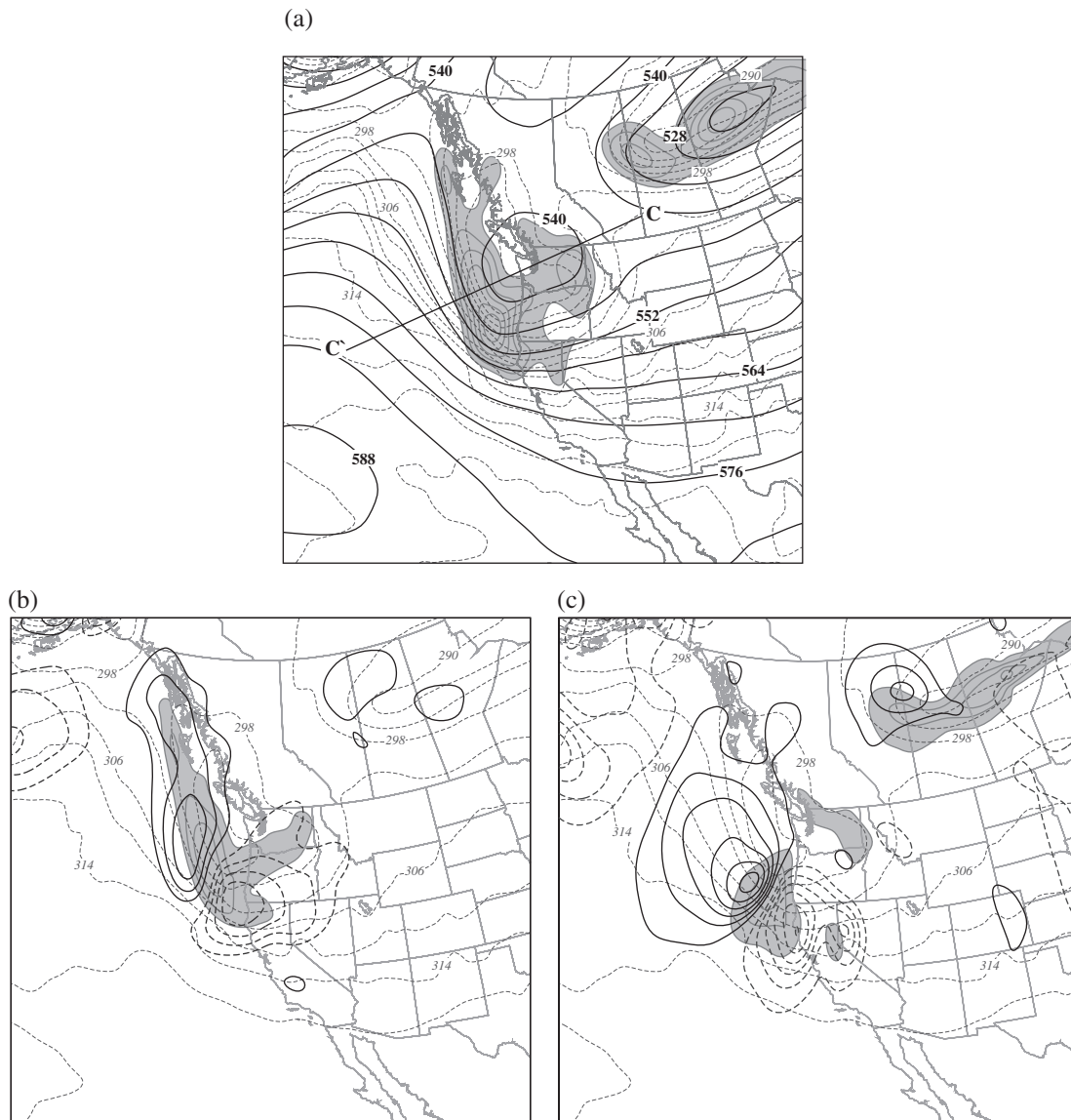


Figure 8. (a) 500 hPa geopotential height (bold solid lines), potential temperature (dashed lines) and geostrophic vorticity (shaded) from NCEP's Global Forecast System (GFS) analysis valid at 0000 UTC 8 April 2013. Vorticity labelled and contoured in units of $4 \times 10^{-5} \text{ s}^{-1}$, beginning at $4 \times 10^{-5} \text{ s}^{-1}$. Geopotential height labelled in m and contoured every 60 m. Potential temperature labelled in K and contoured every 2 K. Vertical cross-sections along line C–C' are shown in Figure 9. (b) 500 hPa geostrophic shear vorticity, potential temperature, and QG ω associated with geostrophic shear vorticity advection by the thermal wind from the GFS analysis valid at 0000 UTC 8 April 2013. Vorticity shaded and contoured as in (a). Potential temperature labelled as in (a) but contoured every 4 K. Solid (dashed) lines are 500 hPa QG ω contoured every 1 (–1) dPa s^{-1} starting at 1 (–1) dPa s^{-1} . (c) As for (b) but for geostrophic curvature vorticity and QG ω associated with geostrophic curvature vorticity advection by the thermal wind.

Oregon/California coast and was distributed more isotropically with its maxima centred on the middle of the upper baroclinic zone (Figure 8(c)).

A series of vertical cross-sections along C–C' in Figure 8(a) are shown in Figure 9. As was the case in the idealized model simulation, the shear vorticity advection forced a narrow subsidence maxima located directly beneath the jet core on the equatorward side of the PV extrusion (Figure 9(a)) which promoted robust tilting frontogenesis within the upper baroclinic zone (Figure 9(b)). Though the QG ω associated with curvature vorticity was broader as in the idealized simulation, the gradients of ω on the cold side of the upper baroclinic zone were much stronger in this observed case (Figure 9(c)). While this difference produced a more robust contribution to tilting frontogenesis (Figure 9(d)), the contribution was focused in the lower stratosphere on the cold side of the developing upper front and did not penetrate as deeply into the upper troposphere as the contribution from shear vorticity. Finally, the transverse QG ω (Figure 9(e)) was displaced to the warm side of the upper baroclinic zone and therefore produced modest tilting

frontogenesis in nearly the same location, and to the same vertical depth, as the shear vorticity contribution though with only about half the vigour (Figure 9(f)).

Development of the upper level jet-front system continued through to 1200 UTC 8 April by which time the magnitude of the 500 hPa temperature gradient had further intensified and the associated geostrophic vorticity strip extended from the central British Columbia coast southward to a robust maximum in southern Nevada (Figure 10(a)). Geostrophic cold air advection characterized nearly the entire southern half of the upper front. The QG ω associated with shear vorticity advection was distributed as before with a quasi-linear band of subsidence along the upper baroclinic zone, the southern portion of which was oriented such that the subsidence maximum was displaced toward the warm side of the front (Figure 10(b)). The corresponding ascent maximum was more isotropic and centred on the southeastern tip of the baroclinic zone where surface cyclogenesis was beginning (not shown). The curvature vorticity ω was also distributed similarly to the prior time with an intense along-front gradient of vertical motion centred on the trough axis

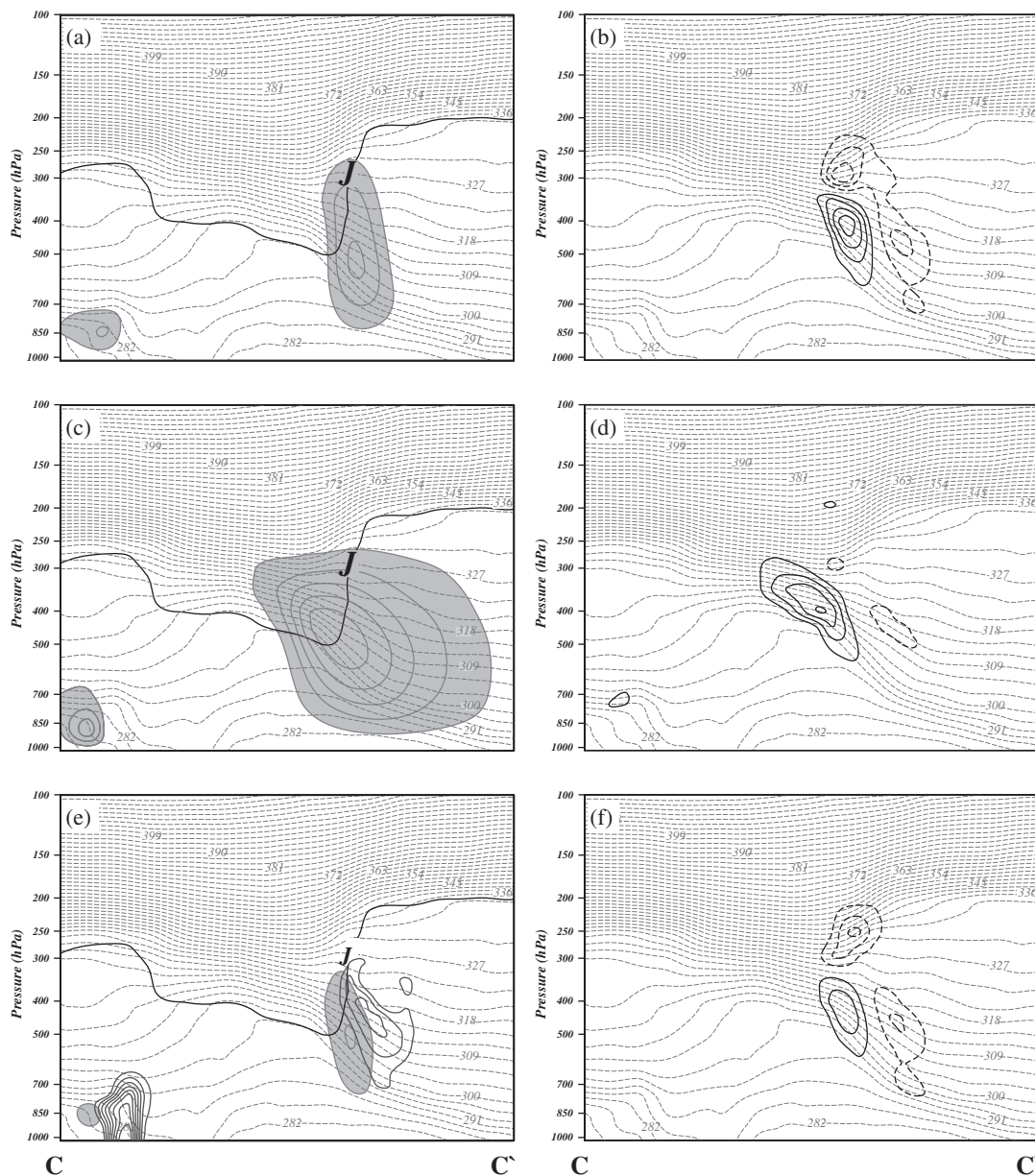


Figure 9. (a) As for Figure 5(a) but along C–C' in Figure 8(a) with data from GFS analysis valid at 0000 UTC 8 April 2013. (b) As for Figure 5(b) but along C–C' in Figure 8(a) with data from the GFS analysis valid at 0000 UTC 8 April 2013. (c) As for Figure 5(c) but along C–C' in Figure 8(a) with data from the GFS analysis valid at 0000 UTC 8 April 2013. (d) As for Figure 5(d) but along C–C' in Figure 8(a) with data from the GFS analysis valid at 0000 UTC 8 April 2013. (e) As for Figure 5(e) but along C–C' in Figure 8(a) with data from the GFS analysis valid at 0000 UTC 8 April 2013. (f) As for Figure 5(f) but along C–C' in Figure 8(a) with data from the GFS analysis valid at 0000 UTC 8 April 2013.

(Figure 10(c)). A stubby axis of maximum subsidence upstream of that location was displaced toward the warm side of the upper front.

Vertical cross-sections along line D–D' in Figure 10(a) are shown in Figure 11. A narrow, frontal-scale region of QG subsidence associated with shear vorticity advection was maximized on the warm side of the upper front, just equatorward of the deep PV extrusion that extended below 700 hPa by this time (Figure 11(a)). This subsidence was responsible for vigorous tilting frontogenesis that extended from the tropopause down to nearly 700 hPa (Figure 11(b)). The weakening of what appears to be a rather robust lower stratospheric front by this subsidence is consistent with the findings of Lang and Martin (2012) concerning lower stratospheric fronts in northwesterly flow. A wider, wave-scale subsidence region was associated with curvature vorticity advection and, as at earlier times in this case, the gradient of subsidence was large on the cold side of the upper baroclinic zone (Figure 11(c)). The corresponding tilting frontogenesis was concentrated at the jet level and was much weaker in the middle

troposphere (Figure 11(d)). Finally, though the transverse QG ω was weak, it was displaced toward the warm side of the upper baroclinic zone (Figure 11(e)) and contributed substantially to tilting frontogenesis along the upper front (Figure 11(f)), though only roughly half as much as the contribution associated with shear vorticity advection.

4. Conclusions

4.1. Summary of results

In both of the cases examined here (as well as in several others perused during the course of this work), the results are essentially the same. The subsidence associated with geostrophic shear vorticity advection by the thermal wind is always distributed in a narrow, quasi-linear frontal-scale column aligned, where geostrophic cold air advection prevails, beneath the jet core and along the warm edge of the upper baroclinic zone. The subsidence associated with geostrophic curvature vorticity advection is often

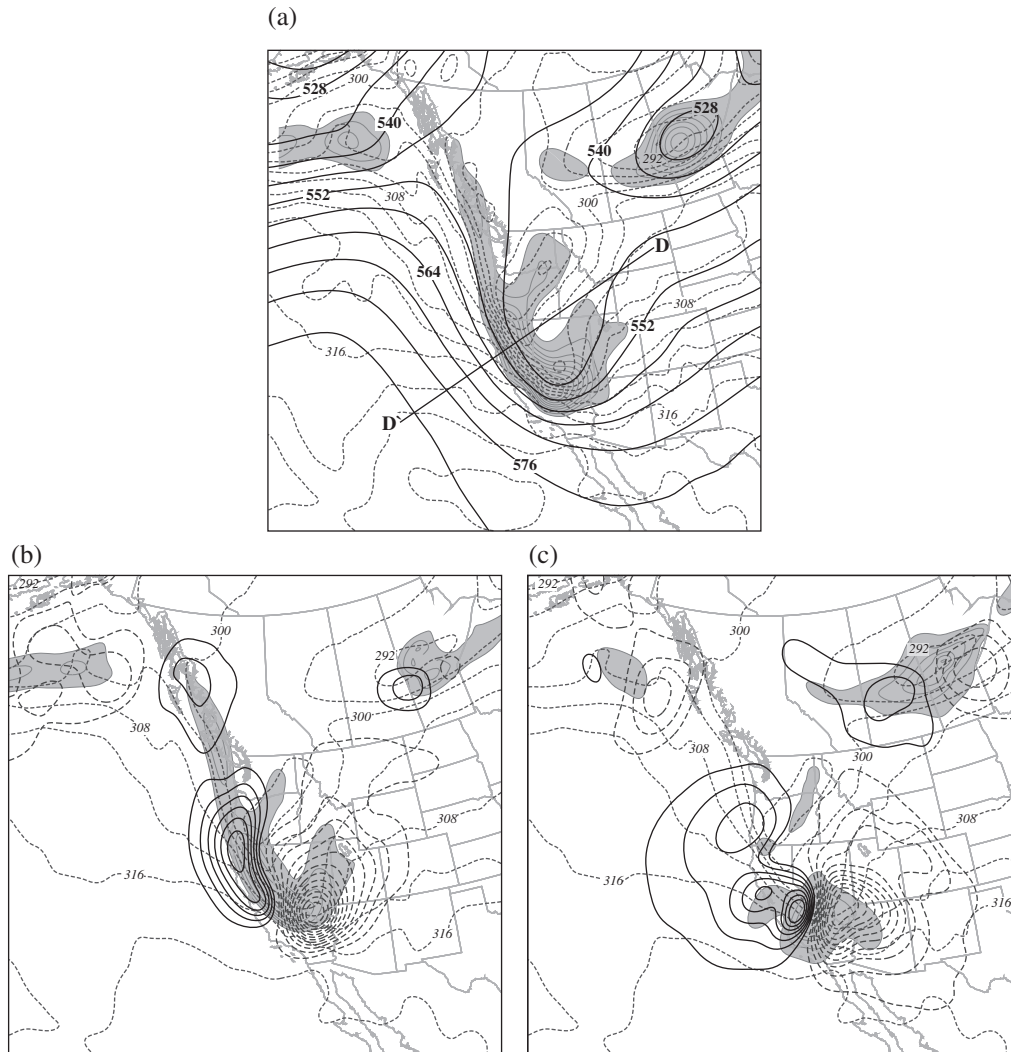


Figure 10. (a) As for Figure 8(a) but from the GFS analysis valid at 1200 UTC 8 April 2013. Vertical cross-sections along line D–D' are shown in Figure 11. (b) As for Figure 8(b) but from the GFS analysis valid at 1200 UTC 8 April 2013. (c) As for Figure 8(c) but from the GFS analysis valid at 1200 UTC 8 April 2013.

of wider horizontal extent, and usually located more nearly in the middle, rather than on the warm side, of the upper baroclinic zone. The couplet of transverse QG ω is, as first recognized by Shapiro (1981), displaced to the warm side of the upper baroclinic zone in regions of geostrophic confluence and shear characterized by geostrophic cold air advection (such as in the northwesterly flow upstream of the upper trough axes in the cases presented here).

The simultaneity of regions of negative vorticity advection increasing with height (i.e. NVA by the thermal wind) and upper tropospheric cold air advection in the upper-frontal environment was first noted by Mudrick (1974) in an idealized simulation of upper frontogenesis. He argued that the subsidence beneath the jet core that characterized developing upper fronts was the result of NVA increasing with height in that column forced by the cross-isobar flow toward lower pressure (i.e. toward the cyclonic shear side of the jet) induced by frontogenetic confluence upstream of an upper trough. Subsidence maximized through the jet core serves to increase the cross-jet vorticity gradient by simultaneously increasing (decreasing) the relative vorticity on the cyclonic (anticyclonic) shear side. Thus a positive feedback between the confluent frontogenesis and NVA-induced subsidence was suggested. Mudrick (1974) further asserted that subsidence through the jet core was enhanced as a result of a maximum of geostrophic cold air advection at and above jet level. His argument referenced a version of the traditional QG omega equation (see his Eq. 11) and was made before Trenberth (1978) demonstrated the connection between that expression and the

Sutcliffe (1947) approximation to it which emphasizes the role of geostrophic vorticity advection by the thermal wind in forcing QG ω . It is now clear that what Mudrick (1974) considered as separate forcings for subsidence actually arise simultaneously out of a common synoptic characteristic of the upper-frontal environment – that is, regions of geostrophic cold air advection in cyclonic shear are always characterized by negative geostrophic vorticity advection by the thermal wind.^{||} The foregoing analysis has demonstrated that this forcing results in banded subsidence through the jet core which promotes frontogenetic tilting and extrusion of stratospheric air into the upper troposphere along the tilted isentropes. Moreover, as demonstrated by the present analysis, this component of the subsidence in the upper frontal environment can exceed that associated with the confluent frontogenetic couplet, the displacement of which (by the presence of lateral shear) toward the warm side of the upper baroclinic zone was not expressly considered by Mudrick (1974) but constitutes the physical aspect of the broader Shapiro effect that has perhaps been overemphasized. The analysis presented here suggests that Mudrick's (1974) emphasis on NVA increasing with height combined with Shapiro's (1981) insight regarding the lateral displacement of frontogenetic transverse circulations is the most

^{||} It should be noted that regions of geostrophic cold air advection in cyclonic (anticyclonic) shear or warm air advection in anticyclonic (cyclonic) shear are always characterized by negative (positive) geostrophic vorticity advection by the thermal wind.

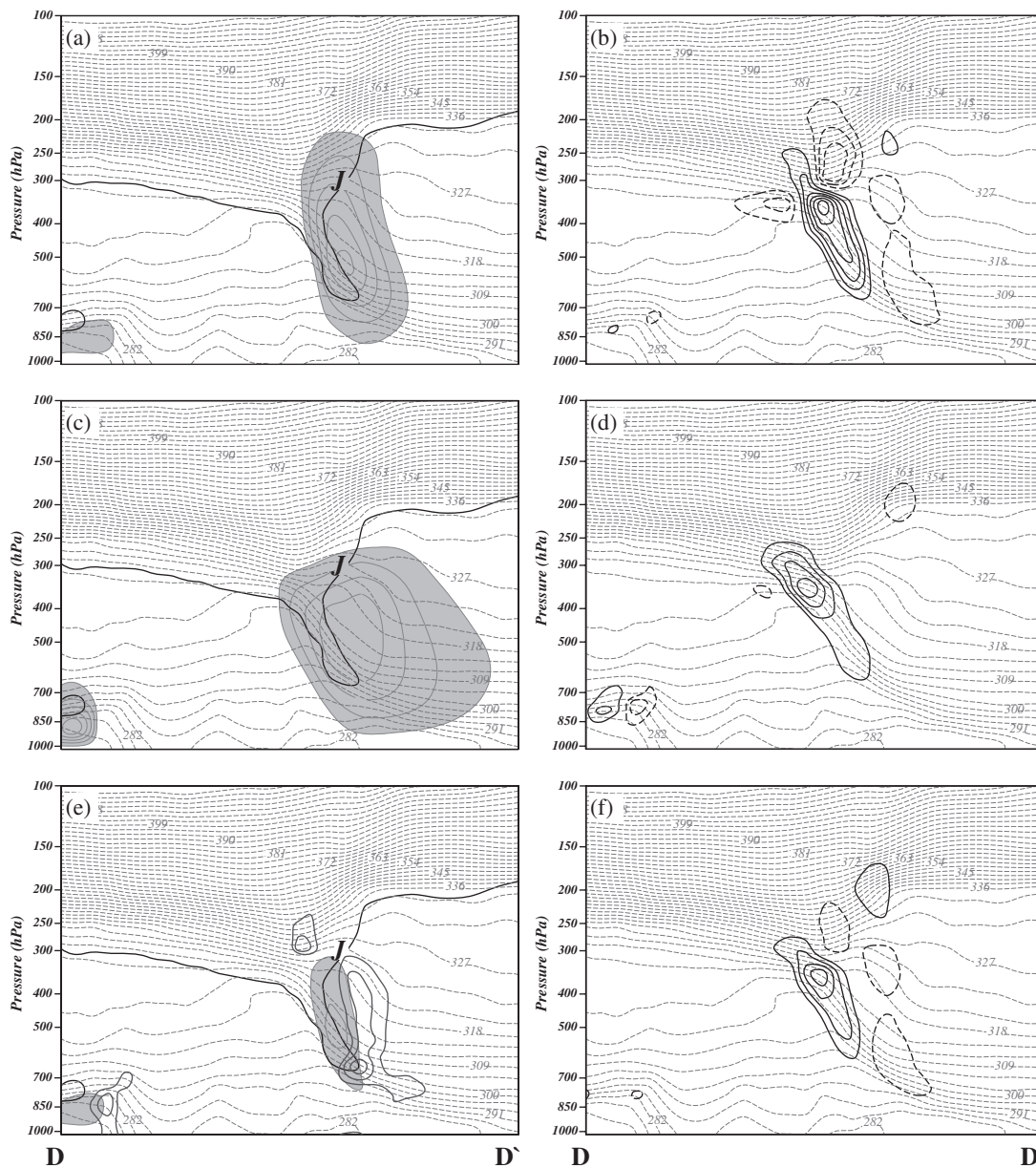


Figure 11. (a) As for Figure 5(a) but along D–D' in Figure 10(a) with data from GFS analysis valid at 1200 UTC 8 April 2013. (b) As for Figure 5(b) but along D–D' in Figure 10(a) with data from the GFS analysis valid at 1200 UTC 8 April 2013. (c) As for Figure 5(c) but along D–D' in Figure 10(a) with data from the GFS analysis valid at 1200 UTC 8 April 2013. (d) As for Figure 5(d) but along D–D' in Figure 10(a) with data from the GFS analysis valid at 1200 UTC 8 April 2013. (e) As for Figure 5(e) but along D–D' in Figure 10(a) with data from the GFS analysis valid at 1200 UTC 8 April 2013. (f) As for Figure 5(f) but along D–D' in Figure 10(a) with data from the GFS analysis valid at 1200 UTC 8 April 2013.

comprehensive way to conceptualize the forcings that promote rapid upper level jet-front development in regions of geostrophic cold air advection in cyclonic shear.

4.2. Discussion

Importantly, the subsidence associated with vorticity advection by the thermal wind is of the shearwise, not transverse, variety. This distinction may have important implications regarding the energetics of upper frontogenesis. Changes in eddy kinetic energy (EKE) are largely controlled by divergence of ageostrophic geopotential flux and baroclinic conversion (Orlanski and Sheldon, 1995). Of these two processes, only baroclinic conversion can generate new EKE through the action of vertical circulations as described by

$$\frac{\partial(EKE)}{\partial t} = -\omega\alpha \tag{6}$$

where ω and α are the perturbation vertical motion and specific volume, respectively. Thus, thermally direct (indirect) vertical circulations convert available potential energy (APE) to EKE (create APE from EKE). Since any species of shearwise QG ω is forced by convergence of an along-isentrope component of the Q-vector, the resulting ω is distributed in couplets oriented along the geostrophic vertical shear. Such a distribution may render shearwise ω less efficient at baroclinic conversion than transverse ω where the updraught/downdraught couplets may be more predisposed to coincidence with perturbation warm or cold air. It is, therefore, possible that the major contributor to tilting frontogenesis (negative geostrophic shear vorticity advection by the thermal wind) may not play the predominant role in the EKE generation required in the development of upper level jet-front systems. More complete investigation of this issue is left for future work.

The analysis presented in this article details the forcings for QG ω that operate in the presence of along-flow geostrophic cold air advection. The present article does not, however, address the

establishment of the along-flow geostrophic cold air advection itself. That question has been considered in a number of previous contributions (e.g. Rotunno *et al.*, 1994; Schultz and Doswell, 1999; Schultz and Sanders, 2002; Lang and Martin, 2013a) and is still at issue. To date, the net result of this debate appears to be verification of the Rotunno *et al.* (1994) notion that along-flow gradients in subsidence upstream of trough axes are of primary importance in establishing along-flow geostrophic cold air advection. Insight into the origin of the necessary along-flow subsidence gradients may be afforded through adoption of the vorticity partition employed in this article. Since the evolution to along-flow geostrophic cold air advection from a state of equivalent barotropy depends entirely upon such subsidence gradients, it is worth considering this special case. Certainly, in such a case, variations of curvature vorticity in a wave train are capable of producing a QG ω pattern in which descent is largest immediately upstream (downstream) of an upper trough (ridge) axis. Consequently, a local minimum in QG ω would likely occur near the inflection point between the upstream ridge and downstream trough. The maximum in curvature-induced ω near the trough (ridge) axis would tend to reorient the isentropes in such a way as to promote geostrophic cold (warm) air advection from the trough axis (ridge crest) to somewhere near the inflection point in the upstream (downstream) northwesterly flow. Such a geostrophic temperature advection pattern is often observed in northwesterly flow (Schultz and Doswell, 1999), as illustrated in the case presented by Lang and Martin (2010) (see their Figs 3 and 4).

On the other hand, shear vorticity advection by the thermal wind in an equivalent barotropic atmosphere would produce a classic four-quadrant pattern in which couplets of vertical motion would straddle the thermal wind at both the entrance and exit regions of jet streaks. Such a distribution of ω would contribute to anticyclonic (cyclonic) rotation of isentropes on the cyclonic (anticyclonic) shear side of the jet (see Eqs 10b and 11b of Schultz and Doswell, 1999). Counteracting these rotations would be the rotation of $\nabla\theta$ on either side of the jet axis provided by the vorticity itself, making establishment of along-flow geostrophic temperature advection difficult to achieve. Thus, it is possible that curvature vorticity advection by the thermal wind, by abetting the establishment of geostrophic cold air advection along the flow, activates the shear vorticity advection by the thermal wind that actually drives the subsidence that folds the tropopause, subducts stratospheric air into the troposphere and intensifies the upper level jet-front system. Systematic consideration of this issue requires diagnosis using output from an appropriate idealized model simulation and is currently underway.

Future work will explore the usefulness of the shear/curvature partition employed here in the examination of additional cyclone life-cycle diagnoses. These efforts will include consideration of the separate circulations associated with shear and curvature PV derived using the piecewise PV inversion scheme of Davis and Emanuel (1991).

Acknowledgement

This research was supported by the National Science Foundation under grant NSF-0950349. The thoughtful comments of two anonymous reviewers are greatly appreciated. Justin McLay provided the idealized UW-NMS simulations. This article is dedicated to the memory of Bro. Robert J. Sullivan, C.F.X., a lifelong friend and mentor to the author.

References

- Barnes SL, Caracena F, Marroquin A. 1996. Extracting synoptic-scale diagnostic information from mesoscale models: The Eta model, gravity waves, and quasigeostrophic diagnostics. *Bull. Am. Meteorol. Soc.* **77**: 519–528.
- Bell GD, Keyser D. 1993. Shear and curvature vorticity and potential-vorticity interchanges: Interpretation and application to a cutoff cyclone event. *Mon. Weather Rev.* **121**: 76–102.
- Bjerknes J, Solberg H. 1922. Life cycles of cyclones and the polar front theory of atmospheric circulation. *Geophys. Publ.* **3**: 1–18.
- Buzzi A, Nanni T, Taglicazucca M. 1977. Mid-tropospheric frontal zones: Numerical experiments with an isentropic coordinate primitive equation model. *Arch. Meteorol. Geophys. Bioklim.* **A26**: 155–178.
- Cao Z, Cho H-R. 1995. Generation of moist potential vorticity in extratropical cyclones. *J. Atmos. Sci.* **52**: 3263–3282.
- Danielsen EF. 1964. 'Project springfield report', DASA 1517. Defense Atomic Support Agency: Washington, DC (DDC).
- Davis CA, Emanuel KA. 1991. Potential vorticity diagnostics of cyclogenesis. *Mon. Weather Rev.* **119**: 1929–1953.
- Eliassen A. 1962. On the vertical circulation in frontal zones. *Geophys. Publ.* **24**: 147–160.
- Fritsch JM, Magaziner EL, Chappell CF. 1980. Analytical initialization for three-dimensional models. *J. Appl. Meteorol.* **19**: 809–818.
- Holton JR. 1979. *An Introduction to Dynamic Meteorology* (2nd edn), *International Geophysics Series* 23. Academic Press: New York, NY.
- Hoskins BJ, Pedder MA. 1980. The diagnosis of mid-latitude synoptic development. *Q. J. R. Meteorol. Soc.* **106**: 707–719.
- Hoskins BJ, Draghici I, Davies HC. 1978. A new look at the ω -equation. *Q. J. R. Meteorol. Soc.* **104**: 31–38.
- Keyser D. 1999. On the representation and diagnosis of frontal circulations in two and three dimensions. In *The Life Cycles of Extratropical Cyclones*, Shapiro MA, Gronas S. (eds.): 239–264. American Meteorological Society: Boston, MA.
- Keyser D, Pecnick MJ. 1985. A two-dimensional primitive equation model of frontogenesis forced by confluence and horizontal shear. *J. Atmos. Sci.* **42**: 1259–1282.
- Keyser D, Shapiro MA. 1986. A review of the structure and dynamics of upper-level frontal zones. *Mon. Weather Rev.* **114**: 452–499.
- Keyser D, Schmidt BD, Duffy DG. 1992a. Quasigeostrophic diagnosis of three-dimensional ageostrophic circulations in an idealized baroclinic disturbance. *Mon. Weather Rev.* **120**: 698–730.
- Keyser D, Schmidt BD, Duffy DG. 1992b. Quasigeostrophic vertical motions diagnosed from along- and cross-isentropic components of the Q vector. *Mon. Weather Rev.* **120**: 731–741.
- Lackmann GM, Keyser D, Bosart LF. 1997. A characteristic life cycle of upper-tropospheric cyclogenetic precursors during the Experiment on Rapidly Intensifying Cyclones over the Atlantic (ERICA). *Mon. Weather Rev.* **125**: 2729–2758.
- Lang AA, Martin JE. 2010. The influence of rotational frontogenesis and its associated shearwise vertical motions on the development of an upper-level front. *Q. J. R. Meteorol. Soc.* **136**: 239–252.
- Lang AA, Martin JE. 2012. The structure and evolution of lower stratospheric frontal zones. Part I: Examples in northwesterly and southwesterly flow. *Q. J. R. Meteorol. Soc.* **138**: 1350–1365.
- Lang AA, Martin JE. 2013a. Reply to comments on 'The influence of rotational frontogenesis and its associated shearwise vertical motions on the development of an upper front'. *Q. J. R. Meteorol. Soc.* **139**: 273–279.
- Lang AA, Martin JE. 2013b. The structure and evolution of lower stratospheric frontal zones. Part II: The influence of tropospheric ascent on lower stratospheric frontal development. *Q. J. R. Meteorol. Soc.* **139**: 1798–1809.
- Martin JE. 1999. The separate roles of geostrophic vorticity and deformation in the mid-latitude occlusion process. *Mon. Weather Rev.* **127**: 2404–2418.
- Martin JE. 2006. The role of shearwise and transverse quasigeostrophic vertical motions in the midlatitude cyclone life cycle. *Mon. Weather Rev.* **134**: 1174–1193.
- Mudrick SE. 1974. A numerical study of frontogenesis. *J. Atmos. Sci.* **39**: 869–892.
- Newton CW. 1954. Frontogenesis and frontolysis as a three-dimensional process. *J. Meteorol.* **11**: 449–461.
- Newton CW, Trevisan A. 1984. Clinogenesis and frontogenesis in jet-stream waves. Part I: Analytical relations to wave structure. *J. Atmos. Sci.* **41**: 2717–2734.
- Nuss WA, Anthes RA. 1987. A numerical investigation of low-level processes in rapid cyclogenesis. *Mon. Weather Rev.* **115**: 2728–2743.
- Orlanski I, Sheldon JP. 1995. Stages in the energetics of baroclinic systems. *Tellus* **47A**: 605–628.
- Pecnick MJ, Keyser D. 1989. The effect of spatial resolution on the simulation of upper-tropospheric frontogenesis using a sigma-coordinate primitive-equation model. *Meteorol. Atmos. Phys.* **40**: 137–149.
- Reed RJ. 1955. A study of a characteristic type of upper-level frontogenesis. *J. Meteorol.* **12**: 226–237.
- Reed RJ, Danielsen EF. 1959. Fronts in the vicinity of the tropopause. *Arch. Meteorol. Geophys. Bioklim.* **A11**: 1–17.
- Reed RJ, Sanders F. 1953. An investigation of the development of a mid-tropospheric frontal zone and its associated vorticity field. *J. Meteorol.* **10**: 338–349.
- Reeder MJ, Keyser D. 1988. Balanced and unbalanced upper-level frontogenesis. *J. Atmos. Sci.* **45**: 3366–3386.

- Rotunno R, Skamarock WC, Snyder C. 1994. An analysis of frontogenesis in numerical simulations of baroclinic waves. *J. Atmos. Sci.* **51**: 3373–3398.
- Sanders F. 1988. Life history of mobile troughs in the upper westerlies. *Mon. Weather Rev.* **116**: 2629–2648.
- Sanders F, Hoskins BJ. 1990. An easy method for estimation of Q-vectors from weather maps. *Weather Forecast.* **5**: 346–353.
- Sawyer JS. 1956. The vertical circulation at meteorological fronts and its relation to frontogenesis. *Proc. R. Soc. A* **234**: 346–362.
- Schultz DM, Doswell CA. 1999. Conceptual models of upper-level frontogenesis in south-westerly and north-westerly flow. *Q. J. R. Meteorol. Soc.* **125**: 2535–2562.
- Schultz DM, Sanders F. 2002. Upper-level frontogenesis associated with the birth of mobile troughs in northwesterly flow. *Mon. Weather Rev.* **130**: 2593–2610.
- Shapiro MA. 1980. Turbulent mixing within tropopause folds as a mechanism of the exchange of constituents between the stratosphere and troposphere. *J. Atmos. Sci.* **37**: 994–1004.
- Shapiro MA. 1981. Frontogenesis and geostrophically forced secondary circulations in the vicinity of jet stream–frontal zone systems. *J. Atmos. Sci.* **38**: 954–973.
- Shapiro MA. 1982. *Mesoscale Weather Systems of the Central United States*. CIRES, University of Colorado/NOAA: Boulder, CO.
- Shapiro MA. 1983. Mesoscale weather systems of the central United States. In *The National STORM Program: Scientific and Technological Bases and Major Objectives*, Anthes RA (ed.): 3.1–3.77. University Corporation for Atmospheric Research: Boulder, CO.
- Stohl A, Bonasoni P, Cristofanelli P, Collins W, Feichter J, Frank A, Forster C, Gerasopoulos E, Gäggeler H, James P, Kentarchos T, Kreipl S, Kolb-Kromp H, Krüger B, Land C, Meloan J, Papayannis A, Priller A, Seibert P, Sprenger M, Roelofs GJ, Scheel E, Schnabel C, Seigmund P, Tobler L. 2003. Stratosphere–troposphere exchange: A review, and what we have learned from STACCATO. *J. Geophys. Res.* **108**: 8516, doi: 10.1029/2002JD002490.
- Sutcliffe RC. 1947. A contribution to the problem of development. *Q. J. R. Meteorol. Soc.* **73**: 370–383.
- Thorncroft CD, Hoskins BJ, McIntyre ME. 1993. Two paradigms of baroclinic-wave life-cycle behaviour. *Q. J. R. Meteorol. Soc.* **119**: 17–55.
- Trenberth KE. 1978. On the interpretation of the diagnostic quasi-geostrophic omega equation. *Mon. Weather Rev.* **106**: 131–137.
- Tripoli GJ. 1992. A nonhydrostatic model designed to simulate scale interaction. *Mon. Weather Rev.* **120**: 1342–1359.
- Uccellini LW, Keyser D, Brill KF, Wash DH. 1985. The Presidents' Day cyclone of 18–19 February 1979: Influence of upstream trough amplification and associated tropopause folding on rapid cyclogenesis. *Mon. Weather Rev.* **113**: 962–988.